Bioactive Materials 16 (2022) 107–119

Contents lists available at ScienceDirect

Bioactive Materials

journal homepage: www.keaipublishing.com/en/journals/bioactive-materials

Remodeling tumor immunosuppressive microenvironment via a novel bioactive nanovaccines potentiates the efficacy of cancer immunotherapy

Xiaoxue Xie [a], Yi Feng [a], Hanxi Zhang [a], Qingqing Su [a], Ting Song [a], Geng Yang [a], Ningxi Li [a], Xiaodan Wei [a], Tingting Li [a], Xiang Qin [a], Shun Li [a], Chunhui Wu [a], Xiaojuan Zhang [c], Guixue Wang [c,***], Yiyao Liu [a,b,**], Hong Yang [a,*]

[a] Department of Biophysics, School of Life Science and Technology, University of Electronic Science and Technology of China, Chengdu, 610054, Sichuan, PR China
[b] TCM Regulating Metabolic Diseases Key Laboratory of Sichuan Province, Hospital of Chengdu University of Traditional Chinese Medicine, No. 39 Shi-er-qiao Road, Chengdu, 610072, Sichuan, PR China
[c] Key Laboratory of Biorheological Science and Technology, Ministry of Education, State and Local Joint Engineering Laboratory for Vascular Implants, Bioengineering College of Chongqing University, Chongqing, 400030, PR China

ARTICLE INFO

Keywords:
Bioactive nanovaccine
Cancer immunotherapy
IDO inhibitor
TAMs
TME

ABSTRACT

The clinical outcomes of cancer nanovaccine have been largely impeded owing to the low antigen-specific T cell response rate and acquired resistance caused by the immunosuppressive tumor microenvironment (TME). Here, we reported a tumor acidity-responsive nanovaccine to remodel the immunosuppressive TME and expand the recruitment of tumor infiltrating lymphocytes (TILs) using hybrid micelles (HM), which encapsulated colony stimulating factor 1 receptor (CSF1-R) inhibitor BLZ-945 and indoleamine 2,3-dioxygenase (IDO) inhibitor NLG-919 in its core and displayed a model antigen ovalbumin (OVA) on its surface (denoted as BN@HM-OVA). The bioactive nanovaccine is coated with a polyethylene glycol (PEG) shell for extending nanoparticle circulation. The shell can be shed in response to the weakly acidic tumor microenvironment. The decrease in size and the increase in positive charge may cause the deep tumor penetration of drugs. We demonstrated that the bioactive nanovaccine dramatically enhance antigen presentation by dendritic cells (DCs) and drugs transportation into M1-like tumor-associated macrophages (TAMs) and tumor cells via size reduction and increasing positive charge caused by the weakly acidic TME. Such bioactive nanovaccine could remodel the immunosuppressive TME into an effector T cells favorable environment, leading to tumor growth inhibition in prophylactic and therapeutic E.G7-OVA tumor models. Furthermore, combining the bioactive nanovaccine with simultaneous anti-PD-1 antibody treatment leads to a long-term tumor inhibition, based on the optimal timing and sequence of PD-1 blockade against T cell receptor. This research provides a new strategy for the development of efficient cancer immunotherapy.

1. Introduction

In recent years, cancer immunotherapy has great potential in enhancing cancer treatment outcomes [1,2]. Among different types of cancer immunotherapy strategies, cancer vaccines have been studied owing to the ability to elicit tumor-specific immune response [3]. Despite cancer vaccines have exhibited promising antitumor efficiency in some cases [4], the therapeutic efficacy is impeded by the rapid clearance of soluble antigen, poor internalization of antigen by antigen-presenting cells (APCs), inefficient maturation of dendritic cells

Peer review under responsibility of KeAi Communications Co., Ltd.
* Corresponding author. Department of Biophysics, School of Life Science and Technology, University of Electronic Science and Technology of China, Chengdu, 610054, Sichuan, PR China.
** Corresponding author. Department of Biophysics, School of Life Science and Technology, University of Electronic Science and Technology of China, Chengdu 610054, Sichuan, P.R. China.
*** Corresponding author. Key Laboratory of Biorheological Science and Technology, Ministry of Education, State and Local Joint Engineering Laboratory for Vascular Implants, Bioengineering College of Chongqing University, Chongqing, 400030, P.R. China.
E-mail addresses: wanggx@cqu.edu.cn (G. Wang), liuyiyao@uestc.edu.cn (Y. Liu), yanghongyh@uestc.edu.cn (H. Yang).

https://doi.org/10.1016/j.bioactmat.2022.03.008
Received 3 January 2022; Received in revised form 1 March 2022; Accepted 3 March 2022
Available online 11 March 2022

(DCs), and poor activation and infiltration of effector T lymphatics. Therefore, it is important to fabricate an antigen carrier that have positive surface charge activation and size reduction in response to endogenous stimuli, which is capable of protecting antigen from degradation and delivering antigens into DCs to activate and expand tumor-specific T cells.

Under the influence of cancer-associated inflammation, the presence of immunosuppressive tumor microenvironment (TME) compromise the antitumor efficiency of cancer vaccine by various negative feedback mechanisms [3]. Indoleamine 2,3-dioxygenase (IDO), involved in the generation of immunosuppressive TME, is a crucial negative feedback enzyme [5,6], that catalyzes the metabolism of essential amino acid L-tryptophan to L-kynurenine [7]. IDO is overexpressed in some cancer cells, resulting in inability to use tryptophan and accumulation of kynurenine in TME, which in turn interferes with the proliferation of effector T cells while promoting the growth of regulatory T cells (Tregs). NLG-919 is an imidazo-isoindoles, which is widely used as a highly IDO-selective inhibitor by blocking IDO mediated immune suppressive pathways.

In addition, tumor-associated macrophages (TAMs), the most substantial tumor-infiltrating immune cells, are commonly affected by TME to differentiate into separate functional phenotypes [8,9]. The M1-like phenotype (M1-like TAMs), defined as classically activated macrophages, induce robust Th1/cytotoxic response by enhancing antigen presentation and stimulating naïve T cells activation [10]. Conversely, the M2-like phenotype (M2-like TAMs), defined as alternatively

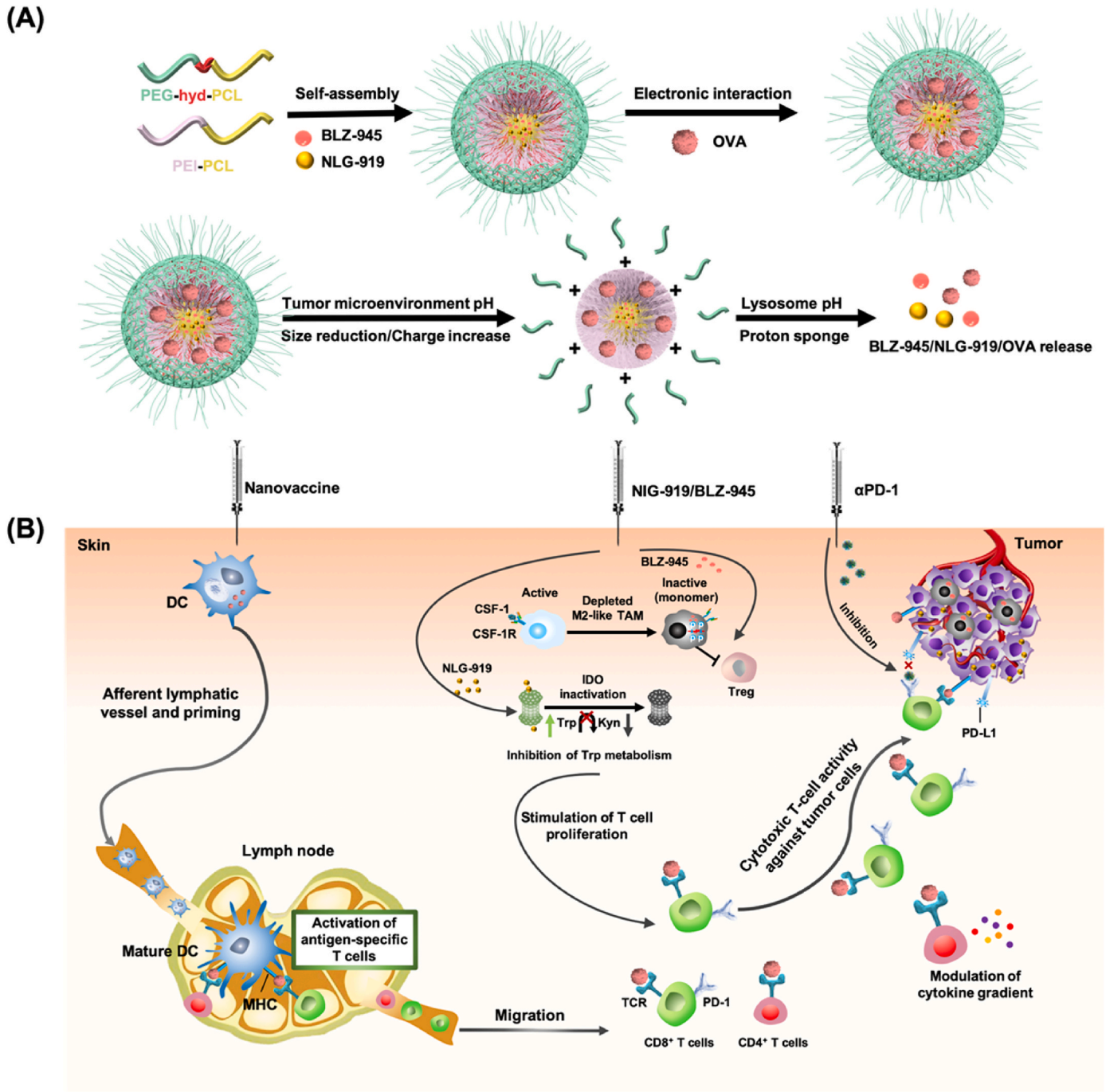

Scheme 1. (A) Synthesis routes of bio-responsive BN@HM-OVA nanovaccine, and the mechanism of drugs/antigen release from hybrid micelles (HM) under acidic pH environment. (B) Graphical illustration for the therapeutic process that combines nanovaccine with BLZ-945/NLG-919 and αPD-1.

activated macrophages, exert pro-tumorigenic activities through facilitating tumor invasion, metastases, angiogenesis and immune escape [11]. M2-like TAMs is another important negative feedback factor contributing to the generation of immunosuppressive TME. Thus, targeting M2-like TAMs is also essential to remodel immunosuppressive TME for improvement of T cell-mediated antitumor immunity. Colony stimulating factor 1 (CSF-1) and its receptor, CSF-1R, which is overexpressed in M2-like TAMs, are viewed as the important pathway for the differentiation and survival of TAMs [12,13]. BLZ-945, a highly selective inhibitor of CSF-1R, directly deplete TAMs by blocking CSF-1R, resulting in reduction in the infiltration of M2-like TAMs and an increase in the infiltration of effector T cells in tumor site. Blockade of these negative regulatory pathways displays a promising strategy for reactivating the antigen-specific immune response caused by cancer vaccines. However, due to the poor solubility of NLG-919 and BLZ-945, their application in therapeutic delivery is greatly limited [14,15]. Therefore, a nanoplatform-based delivery system is essential in accommodating multiple drugs and improving their bioavailability. Based on these observations, it would have important clinical significance to fabricate a novel cancer nanovaccine that could efficiently deliver tumor-associated antigens (TAAs) to DCs, comprehensively alter the immunosuppressive TME into a more beneficial environment for immune cells, and is capable of inducing subsequent T-cell priming and activation to achieve the maximum antitumor responses.

In this work, we reported an orchestrated nanovaccine that has been engineered to remodel the immunosuppressive TME and activate T-cell priming for an effective antitumor immune therapy. This antigen carrier is based on a hybrid micelle (HM) system, which consists of bioresponsive copolymer poly(ethylene glycol)-hydrazone-poly (caprolactone) (PEG-hyd-PCL) linking with a pH-sensitive amide bond, and cationic copolymer poly(ethyleneimine)-poly(caprolactone) (PEI-PCL). Subsequently, BLZ-945 and NLG-919 were encapsulated into the hydrophobic inner core of HM to yield BN@HM. The cationic BN@HM was further utilized for electrostatic adsorption of anionic OVA antigen, which yielded the product of BN@HM-OVA (Scheme 1A). Under weakly acidic tumor microenvironment (pH 6.5–7.0), the positively charged PEI middle layer was exposed owing to the cleavage of PEG layer caused by the fracture of hydrazine. The decreased micelle size and increased positive charge not only can create a "depot effect" at the injection site leading to sustained antigen exposure to DCs, but also enhance the tumor penetration and cellular uptake of BLZ-945 and NLG-919 by M2-like TAMs and tumor cells, respectively. In addition, PEI can facilitate cargo escape owing to the "sponge effect" of PEI in endo/lysosomes (pH 4.5–6.0) after internalization. Then the released exogenous antigens presented by DCs through both MHC-I pathways. Meanwhile, BLZ-945 and NLG-919 were spatiotemporally delivered to intracellular cytoplasm of M2-like TAMs and tumor cells to cause effective M2-like TAMs depletion and suppress IDO activity, respectively. Thus, we hypothesized that BN@HM-OVA could remodel the immunosuppressive TME into an effector T cells favorable environment, which in turn enhance induction of antigen-specific $CD4^+$ and $CD8^+$ T cells infiltration into tumor interiors initiated by OVA antigen, resulting in efficient cancer immunotherapy (Scheme 1B). Considering the integration of programmed cell death protein 1 (PD-1), which overexpressed on T cells, and its ligand, programmed cell death 1 ligand 1 (PD-L1) on tumor cells is detrimental to the therapeutic efficacy of cancer vaccine [16], we further administered the combination of anti-PD1 antibody (αPD-1) and nanovaccine to achieve effective antitumor effect. Notably, the optimal timing and sequence of PD-1 blockade against T cell receptor (TCR) is important to induce beneficial immune response [17]. Finally, we further investigated the combination of cancer vaccine and αPD-1 to overcome resistance and achieve a long-term tumor inhibition.

2. Materials and methods

2.1. Materials

Poly(ethyleneimine)-poly(caprolactone) (PEI_{3k}-PCL_{3k}) and poly (ethylene glycol)-hydrazone-poly(caprolactone) (PEG_{5k}-hyd-PCL_{3k}) were obtained from Xian Ruixi Biological Technology (Xi'an, China). CSF-1R inhibitor BLZ-945 was purchased from MedChemExpress (Monmouth Junction, NJ, USA). IDO targeting agent NLG-919 was purchased from Abmole Bioscience (Houston, USA). $OVA_{257\text{-}264}$ SIINFEKL (OVA_{PEP}) were purchased from Sigma-Aldrich (MO, USA). Roswell Park Memorial Institute 1640 (RPMI-1640), dulbecco's modified eagle medium (DMEM), fetal bovine serum (FBS), penicillin sulfate and streptomycin, L-glutamine, glucose, HEPES, sodium pyruvate, 2-mercaptoethanol, G418 and GM-CSF recombinant mouse protein were obtained from Gibco (Thermo Fisher Scientific, Waltham, MA, USA). Cell Counting Kit-8 (CCK-8) was purchased from Beyotime Biotechnology (Jiangsu, China). ELISA kit was purchased from NeoBioscience (Shenzhen, China). PD-1 monoclonal antibodies were acquired from Bio X Cell (New Hampshire, USA). Other antibodies utilized in this study are listed in the Supplementary Table 1.

2.2. Animals and cells

E.G7-OVA cells, HeLa cells and 4T1 cells were purchased from the Cell Bank of the Chinese Academy of Sciences (Shanghai, China). Female C57BL/6 mice (6–8 weeks) were purchased from Nanjing Biomedical Research Institute of Nanjing University (Nanjing, China). Animal care and experimental procedures were performed in agreement with the guidelines of the Institutional Animal Care Committee of the University of Electronic Science and Technology of China (UESTC). E.G7-OVA cells were cultured in RPMI-1640 medium containing 10% FBS, 1% penicillin sulfate and streptomycin, 2 mM L-glutamine, 4.5 g/L glucose, 10 mM HEPES, 1 mM sodium pyruvate, 50 μM 2-mercaptoethanol and 0.5 mg/mL G418 (Thermo Fisher Scientific, Waltham, MA, USA). Murine bone marrow-derived macrophages (BMDMs) were maintained in DMEM with high glucose containing 10% FBS, 1% penicillin and streptomycin mixture (PS), 1 mM sodium pyruvate, 5 ng/mL GM-CSF recombinant mouse protein. Murine bone marrow dendritic cells (BMDCs) were cultured in RPMI-1640 supplemented with 10% FBS, 1% PS, 20 ng/mL GM-CSF and 10 ng/mL IL-4. All cells were cultured at 37 °C in a humidified atmosphere containing 5% CO_2.

2.3. Preparation and characterization of BLZ-945/NLG-919 and OVA-loaded HM

The BLZ-954/NLG-919 co-loaded hybrid micelles (HM) were prepared using chloroform containing mixture polymer (PEG_{5k}-hyd-PCL_{3k}, 25 mg; PEI_{3k}-PCL_{3k}, 12.5 mg) and BLZ-945 (0.2 mg, dissolved in DMSO) and NLG-919 (3 mg, dissolved in DMSO). After evaporating in a rotary evaporator at 60 °C, the dispersion was added to 70 °C deionized water and further stirred for 1 h at room temperature. Subsequently, the micelles solution was dialyzed against deionized water for 12 h to remove organic solvent with membrane dialysis tubing (molecular weight cutoff of 3.5 kDa, Spectrum Laboratories, Inc. USA) and an ultrafiltration tube (molecular weight of 2K) was used to remove free BLZ-945/NLG-919, resulting BN@HM. Afterwards, 12.5 mg OVA was bounded with PEI through electrostatic adherence by vibrating at 4 °C for 1 h, resulting nanovaccine BN@HM-OVA. The sizes and zeta potentials of the formed BN@HM-OVA nanovaccine were measured with Zetasizer Nano ZS90 (Malvern, UK). The morphology of the nanovaccine was observed with transmission electron microscopy (TEM) (Hitachi, Japan).

2.4. In vitro cellular uptake and intracellular localization of nanovaccines

To examine the cellular uptake of nanovaccines, immature BMDCs

(5×10^5 cells per well) were seeded in confocal dishes and stimulated with BN@HM-OVA-FITC (FITC-labeled OVA, 25 μg/mL) for 2 and 6 h in medium with various pH values (7.4 and 6.8). After washing the spare nanovaccine, BMDCs were harvested and then labeled with Dil to quench the extracellular fluorescence. After washing three times, the cellular internalization of nanovaccine was obtained utilizing a confocal laser scanning microscope (CLSM) (Leica SP5II, Germany).

The lysosome escape behavior of nanovaccine was investigated by CLSM. Immature BMDCs (1×10^6 cells per well) were plated in confocal dishes and then incubated with BN@HM-OVA-FITC (FITC-labeled OVA, 25 μg/mL) in medium with various pH values (7.4 and 6.8). After the designated incubation time points (6 and 36 h), BMDCs labeled with Dil were washed with PBS and then stained with LysoBlue (KeyGEN BioTECH, China). The co-localization degree of lysosomes was determined utilizing a confocal laser scanning microscope (Leica SP5II, Germany).

2.5. Evaluation of IDO enzymatic activity

The inhibitory effect of NLG-919 on IDO enzyme activity was evaluated by HeLa cell-based kynurenine (Kyn) assay [18]. Specifically, HeLa cells (1×10^4 cells per well) were seeded in a 96-well plate and allowed to grow overnight. Interferon-γ (IFN-γ, 50 ng/mL) was added to each well to stimulate the expression of IDO. At the same time, BN@HM-OVA with various concentrations of NLG-919 (NLG919 concentrations: 0–30 μM) was added to cells. After incubation for 48 h, 150 μL of the supernatant from each well was collected to incubate with trichloroacetic acid (75 μL, 30%) at 50 °C for 30 min to hydrolyse N-formylkynurenine to kynurenine. Subsequently, the mixture was incubated with an equal volume of Ehrlich reagent (2% p-dimethylamino-benzaldehyde w/v in glacial acetic acid) for 10 min at room temperature. Reaction product was measured at 490 nm using a microplate reader.

2.6. Study of T cell proliferation

A lymphocyte-HeLa cells co-culture system was performed to determine whether BN@HM-OVA can reverse the inhibition of T cell proliferation caused by IDO [19]. The lymphocytes generated from C57BL/6 mice spleen were seeded in a 96-well plate at a density of 5×10^4 cells per well and cultured in medium containing 100 ng/mL anti-CD3 antibody (eBioscience, Thermo Fisher Scientific) and 10 ng/mL human recombinant interleukin-2 (IL-2, R&D Systems, Shanghai, China) for 3 days. After incubation for 3 days, lymphocytes were stained with CellTraceTM CFSE dye (ThermoFisher Scientific). The HeLa cells (1×10^4 cells per well) were stimulated with IFN-γ for 48 h and then co-cultured with lymphocytes. Various formulations of PBS, HM, free NLG-919 (20 μM), free BLZ-945 (1 μM), free OVA (25 μg/mL) and BN@HM-OVA having the same concentration of drugs and antigen were added to the co-culture system. After 3 days co-culture, T cell proliferation was measured by flow cytometric analysis (Beckman).

2.7. In vitro maturation and T cell priming of BMDCs

For *in vitro* BMDCs maturation assessments, immature BMDCs (5×10^5 cells per well) were seeded in 12-well plates and cultured with PBS, HM, NLG-919 (20 μM), free BLZ-945 (1 μM), free OVA (25 μg/mL) or BN@HM-OVA having same concentration of drugs and antigen for 24 h. BMDCs were subsequently collected and stained with the fluorophore-labeled antibodies against CD11c, CD86, CD80 and CD40 at 30 °C for 30 min. After centrifuging and washing, BMDCs were analyzed by flow cytometry.

To evaluate the priming of T cells, a transwell cell co-culture model was constructed. Briefly, E.G7-OVA (1×10^5 cells per well) cells were cultured in the upper chamber while immature BMDCs (5×10^5 cells per well) were cultured in the lower chamber, both of them were treated with PBS, HM, NLG-919 (20 μM), free BLZ-945 (1 μM), free OVA (25 μg/mL) or BN@HM-OVA having the same concentration of drugs and antigen for 24 h. Then the treated BMDCs were mixed with T lymphocytes isolated form C57BL/6 mice spleen at a BMDCs to T cells ratio of 1:5 to stimulate the activation of T cells. After 48 h of incubation, the cells were collected and stained with fluorophore-labeled antibodies against CD3, CD4 and CD8 at 30 °C for 30 min. After centrifuging and washing, the cells were analyzed by flow cytometry.

2.8. Immunization of animals with nanovaccines

For the prophylactic combination study, C57BL/6 (8-week old) mice were randomized into six groups ($n = 5$ biologically independent mice for each group) and no criteria for screening animals were set during the experiment. Different treatments (Saline, Free OVA, HM-OVA, 20 μg OVA per mouse for each injection) were intradermally injected into both footpads at the indicated time points for the prophylactic and intervention combinatorial studies in the absence or presence of BLZ-945/NLG-919 (in the formulation of B@HM/N@HM/BN@HM) intertumoral injection (Fig. 4A). Briefly, three weeks after the final vaccination, the immunized mice were subcutaneously inoculated with 3×10^5 E G7-OVA cells. After incubation of tumors for 6 days, B@HM/N@HM BN@HM was administered intratumorally (BLZ-945, 1 mg/kg for each injection; NLG-919, 2 mg/kg for each injection). The tumor volume was measured every other day according to following the formula: V = length × width [2] × 0.5 (mm^3). Mice were euthanized when the average tumor volume reached the ethical endpoint (~2000 mm^3).

2.9. Antitumor efficacy

To analyze the therapeutic efficacy of the formulated nanovaccine in reducing tumor volume, C57BL/6 (8-week old) mice were subcutaneously inoculated with 3×10^5 E G7-OVA cells. When the average tumor volume reached ~50 mm^3, the mice were randomly divided into eight treatment groups ($n = 5$ biologically independent mice for each group) and respectively injected with (1) Saline, (2) HM-OVA, (3) N@HM, (4) N@HM-OVA, (5) B@HM, (6) B@HM-OVA, (7) BN@HM, and (8) BN@HM-OVA every 4 days for three times (OVA, 25 μg per mouse for each injection; BLZ-945, 1 mg/kg for each injection; NLG-919, 2 mg/kg for each injection). The tumor volume was determined according to following the formula: V = length × width [2] × 0.5 (mm^3) and body weight was monitored every other day. Mice were euthanized when the average tumor volume reached the ethical endpoint (~2000 mm^3).

The antitumor efficacy of the combined immunotherapy of BN@HM-OVA with anti-PD-1 was evaluated using two treatment regimens (a simultaneous treatment regimen and a sequential treatment regimen) by varying the sequence of administration of anti-PD-1 antibody (αPD-1; BioXcell; clone: RMP1-14). C57BL/6 (8-week old) mice were subcutaneously inoculated with 3×10^5 E G7-OVA cells. When the average tumor volume reached ~50 mm^3, the mice were injected with BN@HM-OVA nanovaccine (OVA, 25 μg per mouse for each injection; BLZ-945, 1 mg/kg for each injection; NLG-919, 2 mg/kg for each injection) every 4 days for three times. To assess the feasibility of simultaneous treatment regimen, intertumoral injection of αPD-1 (10 mg/kg for each injection) started a day after the first immunization and continued every other day for a total of 6 times. As for the analyze of sequential treatment regimen, mice were intratumorally injected with αPD-1 (10 mg/kg for each injection) every other day for a total of 6 times from 1 week after the last immunization. At the endpoint, tumor-bearing mice were photographed and tumor tissues were removed, weighed, photographed, and flow cytometric analyzed. For each experimental group, any animals, experimental units, or data that were not excluded from this study.

2.10. Flow cytometry

For the assessment of tumor-infiltrating lymphocytes after the above-

mentioned therapy, tumor tissues were isolated from E.G7-OVA tumor-bearing mice and then divided into small pieces, digested and filtered to obtain single-cell suspension. Cells were subsequently stained with fluorescence-labeled antibodies as described in Supplementary Table 1. For example, incubate a single-cell suspension with anti-CD16/32 and then stained with anti-CD11b-BB515, anti-F4/80-PE, anti-CD80-PE-Cy7 and anti-CD206-APC for 30 min at 4 °C.

2.11. ELISA assay

The plasma levels of IFN-γ, TNF-α, IL-6, IL-10 and IL-12 were determined with ELISA kits (NeoBioscience, China) according to the manufacturer's instructions. Briefly, serum samples were separated from mice after different treatments and diluted for analysis.

2.12. Statistical analysis

Animal data are presented as mean ± standard deviation (SD) and other data are shown as mean ± standard error of mean (SEM). Groups were compared by one-way analysis of variance (ANOVA) with post hoc Tukey's test or two-tailed Student's *t*-test using GraphPad Prism software package (PRISM 8.0, GraphPad Prism Software). Statistical significance was defined as $p < 0.05$.

3. Results and discussion

3.1. Synthesis and characterization of nanovaccines

The pH-responsive hybrid micelle (HM) was synthesized with copolymers of PEG-hyd-PCL and PEI-PCL at a mass ratio of 2:1 by film hydration method as reported previously [20]. The structure of PEG-hyd-PCL at different pH were determined by ^{1}H NMR (Fig. S1), which shows that acidic conditions lead to the cleavage. After incubation at various pH values, the obtained HM was analyzed by TEM and zeta potential measurements to confirm the pH-dependent transition of HM. TEM images showed a spherical morphology of HM (Fig. 1A) with a hydrodynamic particle size of 73.5 nm (Fig. 1B) at pH 7.4 (simulation normal tissues). The size of HM drastically decreased to 49.0 nm after incubation at pH 6.8 (simulation tumor microenvironment) analyzed by dynamic light scattering (DLS), which was consistent with the TEM images. Moreover, the surface charge of HM increased from around +19.9 to +26.5 mV (Fig. 1C). These observations suggested that PEG-hyd-PCL were sensitive to weakly acidic pH, and the fragmented PEG would reduce HM size while simultaneously exposing the highly positive-charged PEI. Moreover, after incubation at pH 5.0 (simulated lysosomes), there is almost no complete structure of HM, and its surface potential further increased to about +31.8 mV. The phenomenon could be explained by the protonation of PEI upon acidic pH and the hydrophobicity of PCL.

On the basis of the desirable characteristics of HM, NLG-919 and BLZ-945 were encapsulated into the hydrophobic cores to construct BN@HM, which showed high encapsulation efficiency (EE) and drug loading (DL) (Supplementary Table 2). For NLG-919, EE = 87.03% and DL = 6.1%, whereas for the BLZ-945, EE = 93.06% and DL = 6.5% (Supplementary Table 3). These micelles exhibited a spherical structure (Fig. 1E) with an average diameter of 80.8 nm and a zeta potential of +19.3 mV (Fig. 1D). Subsequently, OVA antigens were loaded on the surface at a mass ratio 1: 1 of OVA to PEI-PCL through electrostatic adherence to form BN@HM-OVA, which exhibited a much rougher surface with clear attached particles (Fig. 1F), an increased average diameter of 94.9 nm and lower zeta potential of +5.9 mV, suggesting that OVA was successfully loaded onto the BN@HM surfaces. Moreover, the morphology of BN@HM-OVA in various pH values indicates the uniformity of nanovaccines and the same acid sensitivity as HM

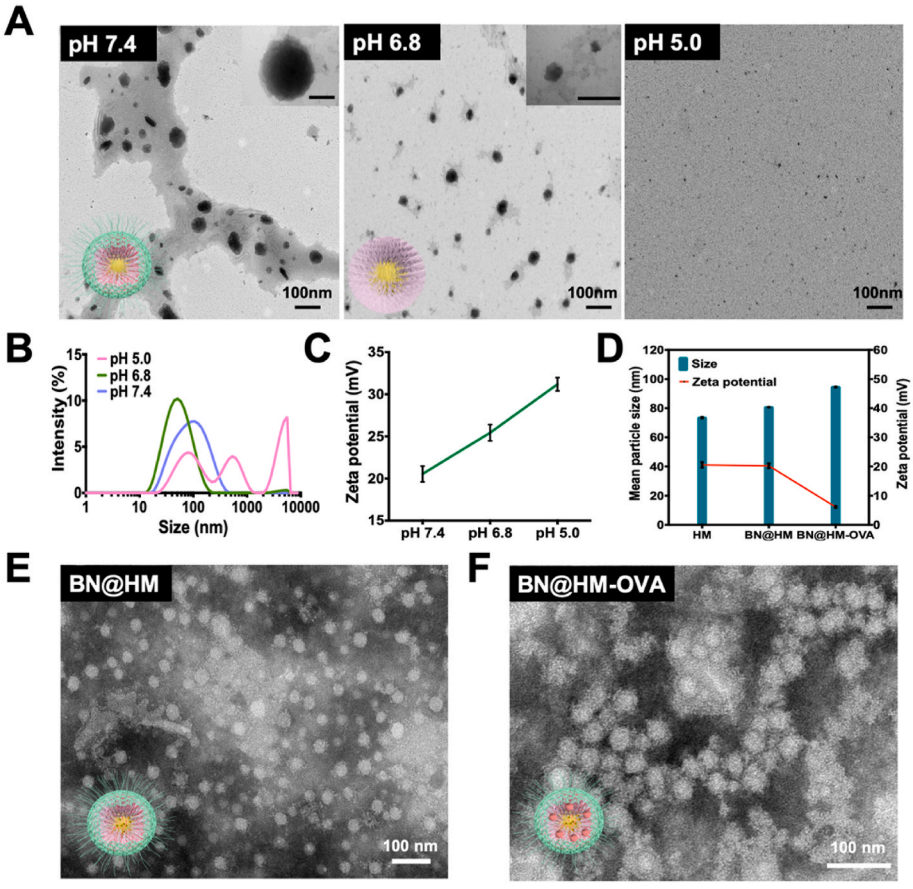

Fig. 1. Characterization of nanovaccines. (A) Representative transmission electron microscopy images, size distribution (B) and zeta potential change (C) of HM after various treatments with pH 7.4, pH 6.8 and pH 5.0 for 4 h. Data are presented as means ± SEM. (n = 3 independent samples). Scale bar = 100 nm; (D) Particle size and zeta potential of HM, BN@HM, BN@HM-OVA, respectively. Data are presented as means ± SEM. (n = 3 independent samples). (E) Representative transmission electron microscopy images of BN@HM and BN@HM-OVA (F). Scale bar = 100 nm.

(Fig. S2). The EE of OVA was about 91.58%, which corresponds to a DL of 14.82%. Furthermore, the antigens and encapsulated BLZ-945/NLG-919 release behavior of BN@HM-OVA was determined by BCA assay and HPLC, respectively. Specifically, around 60% of OVA was released within 48 h (Fig. S4). NLG-919/BLZ-945 was released in a gradual and slow manner at pH 7.4 (Fig. S3). In contrast, the faster BLZ-945/NLG-919 release was observed at pH 5.0, which is affected by the removal of PEG corona and protonation of PEI, suggesting the pH-responsiveness of BN@HM-OVA for controllable drug release.

3.2. Cytotoxic activity, tumor penetration and cellular uptake of nanovaccines

The cytotoxicity of the BN@HM-OVA nanovaccine was investigated by CCK-8 assay. The nanovaccine displayed good cytocompatibility after incubation with BMDCs (Fig. S5A) and E.G7-OVA cells (Fig. S5B) for 48 h, suggesting an excellent biocompatibility of the formulated nanovaccine. Considering fluorescent probes have been used to analyze the intracellular pH change in cancer cells [18], a FRET pair (Dox and Cy5) was loaded into hybrid micelles (donated as DC@HM-OVA) to monitor the penetration of nanovaccine. Furthermore, recording of the excitation and emission spectra for free Dox and Cy5 verified them as the suitable pair to establish FRET system, where the emission wavelength of donor Dox was determined nearly 625 nm, which is almost coincided with the excitation wavelength of acceptor Cy5 (Fig. S6A) [19]. In addition, the FRET spectra of aqueous DC@HM-OVA were obtained by irradiating the suspensions at 485 nm corresponding to the excitation wavelength of the FRET donor of Dox. As pH decreased, sequential decrease in the emission of Cy5 was observed due to a decrease in FRET efficiency (Fig. S6B), indicating less energy transferred from Dox to Cy5, which was consistent with the above-mentioned pH-triggered dissociation of colloidal complex. To investigate the tumor penetration of nanovaccine *in vitro*, multicellular spheroids (MCs) established by 4T1 cells were utilized to simulate solid tumors. MCs were then incubated with DC@HM-OVA for distinct durations at various pH values and dual emission-based fluorescence imaging was visualized by CLSM in optical windows between 560-600 nm and 660–700 nm when irradiating suspensions with 488 nm laser light. As shown in Fig. S7, only a little blue fluorescence (Cy5 imaging channel) was observed in the periphery area of MCs at pH 7.4 after incubation for 4 h, indicating a limited penetration of DC@HM-OVA. After 8 h incubation, blue fluorescence accompanied by the increase of intensity was observed at the cell layers outside MCs, while no red fluorescence (Dox imaging channel) was observed, FRET on with high efficiency in MCs. In addition, both blue fluorescence accompanied by the decrease of intensity and red fluorescence were detected after incubation for 24 h, implying that the efficiency of FRET from Dox to Cy5 decreased relatively due to the swelling of DC@HM-OVA caused by the weakly acidic environment of cancer cells. In contrast, only strong blue fluorescence was observed widely spread within MCs at pH 6.8 after incubation with DC@HM-OVA for 4 h, suggesting the increase of surface potential caused by the removal of PEG segment enhanced tumor penetration of nanovaccine. Moreover, with time progressing, the blue fluorescence became dim but the intensity of red fluorescence obtained from the Dox imaging channel became stronger (FRET off), indicating that Dox and Cy5 were released from micelleplexes (thus an increased distance between each other) and penetrated throughout the whole MCs. In addition, the co-location coefficient of Dox in MCs suggests that after 24 h incubation, compared with pH 7.4 treatment group, broader and stronger distribution of Dox fluorescence was observed at pH6.8. The above results clarified that size reduction and positive charge increase of micelleplexes triggered by pH condition contributed to the improvement of tumor penetration.

Dendritic cells (DCs) are an essential antigen present cells, and antigen uptake by DCs plays an important role in vaccine-elicited antitumor immune responses [21,22]. To determine whether the constructed BN@HM-OVA-FITC nanovaccine can facilitate antigen uptake, the intracellular localization of OVA-FITC in BMDCs labeled with Dil (red fluorescence) was investigated using CLSM. Respective confocal images clearly showed that BN@HM-OVA-FITC could be effectively uptake by BMDCs in a time-dependent manner under the condition of pH 7.4 and 6.8 after 2 and 6 h of incubation (Fig. 2A). Furthermore, regardless of the incubation time, the higher amount of nanovaccine was internalized by BMDCs at pH 6.8 than that at pH 7.4, confirming that the increase in positive charge and the decrease in size property of nanovaccine in response to weakly acidic pH had strong capability to enhance antigen uptake by DCs.

After internalization by BMDCs, nanovaccine was generally trapped in endo/lysosome, which consequently prevented the presentation of exogenous antigen to MHC I molecules. Sequentially, the endo/lysosomal escape capability of BN@HM-OVA-FITC nanovaccine was investigated by CLSM. After 6 h incubation, obvious dotted green fluorescence (OVA-FITC) was found mostly in lysosomes, proved by the well-overlapped green, red (Dil) and blue fluorescence (Lysotracker blue). Meanwhile, the green fluorescence was gradually separated from blue-marked lysosomes after incubation for 12–24 h, suggesting an efficient endosomal escape facilitated by the proton buffering of PEI. These observations indicated the BN@HM-OVA nanovaccine would collapse and release antigen after cell entry, which was beneficial for antigen presentation by DCs.

3.3. T cell proliferation, DCs maturation, T cell priming and cellular phagocytosis induced by nanovaccine in vitro

Inhibition of indoleamine 2,3-dioxygenase (IDO) activity was chosen as a means to remodel the immunosuppressing microenvironment due to the degradation of tryptophan (Trp) into kynurenine (Kyn) catalyzed by IDO impairing the survival and the activity of immune cells [6,23]. The inhibitory IDO activity of BN@HM-OVA was analyzed by the potency of Kyn in inhibiting the conversion of Trp to Kyn in HeLa cells [24]. HeLa cells were treated with IFN-γ to induce IDO expression, followed by the treatment with BN@HM-OVA at various concentrations of NLG-919, and the amount of Kyn in culture medium was determined by a colorimetric assay. IDO activity inhibited by BN@HM-OVA nanovaccine in a concentration-dependent manner (Fig. S8). With the depleting of IDO enzyme, T cells can proliferate to enhance anti-tumor immune responses [25]. Subsequently, the proliferation of splenocytes isolated from C57BL/6 mice spleen was then examined in a vitro lymphocyte-HeLa cells (pretreated with IFN-γ to induce IDO expression) co-culture model (Fig. 3A). In brief, each additional peak, shown in pink (Fig. 3B), suggests one subsequent generation of divided T cells. Lymphocyte/HeLa cells without treatment or treated with HM, the percentage of T cell proliferation is 17.1% and 19.7%, respectively. In addition, the lymphocyte/HeLa cells treated with NLG-919 and BN@HM-OVA have near 30.0% of T cell proliferation, which is higher than the results from other groups, indicating that BN@HM-OVA nanovaccine can effectively stimulate the proliferation of T cells.

Promoting the maturation of dendritic cells (DCs) is critical for antigen presentation and the generation of antigen-specific immune responses [26–28]. As shown in Fig. 3C and Fig. S9,10) , BMDCs treated with BN@HM-OVA nanovaccine showed the highest expression proportions of co-stimulatory molecules CD40, CD80 and CD86, which are typical surface markers of maturated DCs, compared with other groups. Subsequently, an *in vitro* T cell priming assay was used to evaluate the initiation of subsequent immune responses induced by mature BMDCs [29]. Immature BMDCs/E.G7-OVA cells (5:1) pre-treated with various treatments in a transwell cell co-culture system, and then the treated BMDCs were mixed with T lymphocytes (1:5) to stimulate the activation of T cells (Fig. 3D). The flow cytometric analysis results suggested that the percentage of $CD3^+CD4^+$ and $CD3^+CD8^+$ T cells were high to 52.6% and 59.7%, respectively, in the group treated with BN@HM-OVA nanovaccine (Fig. 3E-**F** and Fig. S10). These results indicated that BN@HM-OVA had superiority in DCs maturation which further induce

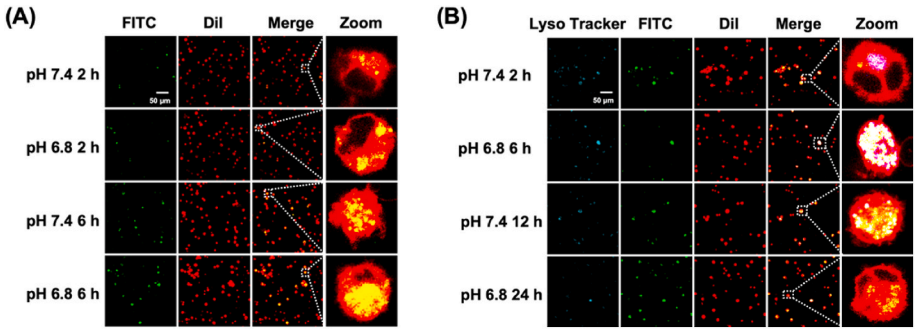

Fig. 2. Uptake of BN@HM-OVA-FITC by BMDCs *in vitro*. (A) Representative confocal fluorescence images of bone marrow-derived dendritic cells (BMDCs) after incubation with BN@HM-OVA-FITC (green) for 2 h and 6 h at pH 7.4 and pH 6.8, respectively. BMDCs were labeled with Dil (red). Scale bars = 50 μm. (B) Representative confocal fluorescence images of BMDCs after incubation with BN@HM-OVA-FITC (green) for 2–24 h at pH 7.4 and pH 6.8, respectively, in which endosomes/lysosomes were stained with Lysotracker (blue) and BMDCs were labeled with Dil (red). Scale bars = 50 μm.

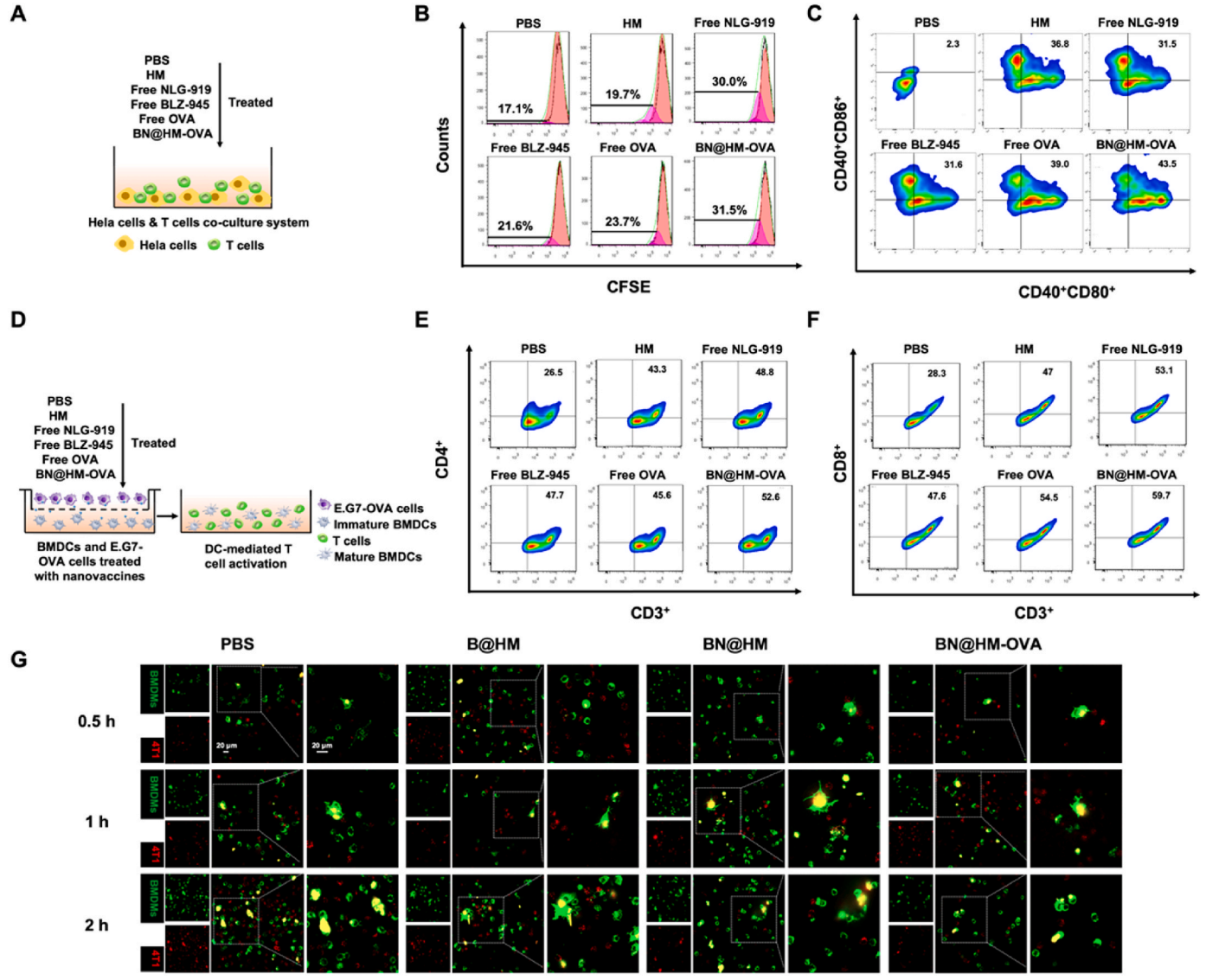

Fig. 3. *In vitro* immune stimulation effect of nanovaccines. (A) Schematic illustration of the measurement of T cell proliferation in a lymphocyte-HeLa cells co-culture system. (B) Representative flow cytometric analysis showing proliferating (carboxyfluorescein succinimidyl ester (CFSE) dilution) $CD3^+$ T cells after incubation in the lymphocyte-HeLa cells co-culture system pulsed with PBS, HM, free NLG-919, free BLZ-945, free OVA and BN@HM-OVA. (C) Representative flow cytometric analysis of $CD80^+CD86^+$ bone marrow-derived dendritic cells (BMDCs) gating on $CD11c^+CD40^+$ cells through flow cytometry after various treatments in (B). (D) Schematic illustration of the transwell system. Briefly, the tumor cells were cultured in the upper chamber while immature BMDCs were cultured in the lower chamber, and both of them were treated with various treatments in (B) for 24 h. Then suspensions of tumor cell lysate and mature BMDCs were co-cultured with T lymphocytes to stimulate the activation of T cells for 48 h. (E) Representative flow cytometric analysis of $CD3^+CD4^+$ lymphocytes (Ths) and (F) $CD3^+CD8^+$ lymphocytes (CTLs). (G) Representative confocal images of M1-polarized macrophages phagocytosis assays, in which M1-like bone-marrow-derived macrophage cells (BMDMs) pre-treated with PBS, B@HM, BN@HM, BN@HM-OVA were stained with DiO (green) and 4T1 cancer cells were stained with CellTracker DeepRed (red). Then M1-like BMDMs were co-cultured with 4T1 cells for 0.5, 1 and 2 h. Scale bar = 20 μm.

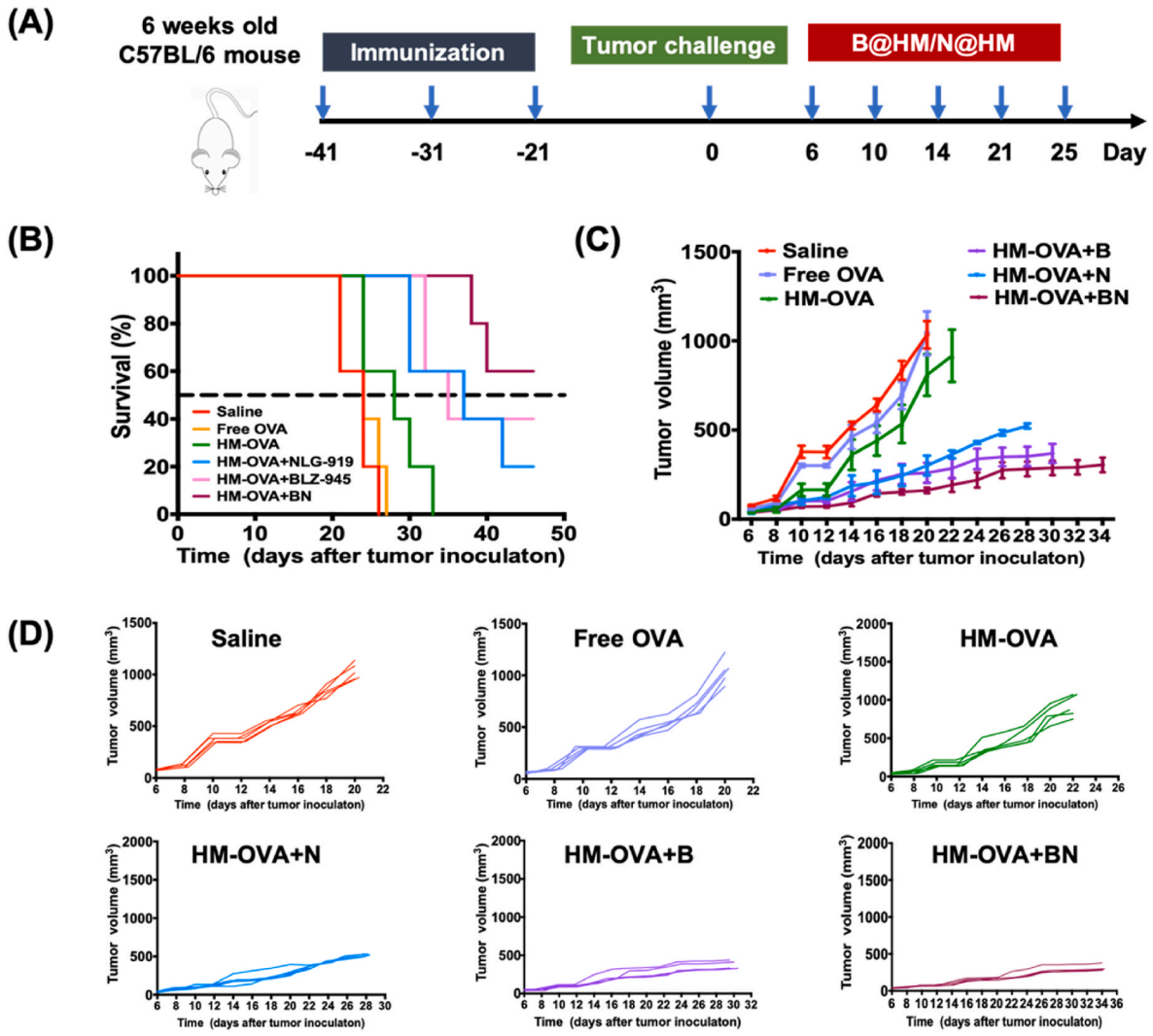

Fig. 4. Prophylactic nanovaccine have a synergistic effect with BLZ-945 and NLG-919, which inhibits tumor growth and prolongs survival in tumor-bearing mice. (A) Scheme of tumor prevention experiment design. (B) Kaplan-Meier overall survival graph for different groups of mice after various treatments. (n = 5 biologically independent mice for each group). (C) Average tumor growth curves (n = 5 biologically independent mice for each group). (D) Individual tumor growth curves in (C). Data are presented as mean ± SD.

the antigen-specific T-cell responses efficiently.

CSF-1R, which is mainly expressed by macrophages and monocytes (macrophage precursor), is recognized as the primary factor for their function maintenance [13,30]. Moreover, recent studies have proved that M2 macrophages expressed a higher amount of CSF-1R than M1 macrophages. Therefore, treatments targeting CSF-1R are highly M2-like TAMs specific [31,32]. Furthermore, confocal images demonstrated that BN@HM-OVA containing BLZ-945 could not impair the phagocytosis of cancer cells by M1-polarized macrophages *in vitro* (Fig. 3G and Fig. S10). Considering myeloid-derived suppressor cells (MDSCs) could be repolarized by PEI from M2 to M1 phenotype [33], BN@HM-OVA enhanced phagocytosis of cancer cells by macrophages and activated innate immune systems.

3.4. The ability of nanovaccine on transportation of antigen to lymph nodes and the prophylactic effects on tumor growth

Lymph nodes (LNs) are the sites where antigen presenting cells (APCs) such as DCs and macrophages take up antigens and the activated DCs met with naïve T cells to facilitate T cell cross-priming [34,35]. To assess whether the nanovaccine migrated to LNs after subcutaneously injected into the footpads, near infrared dye DIR was encapsulated into the core of nanovaccine to yield DIR@HM-OVA. The nanovaccine migrated to draining lymph nodes after injection for 4 h and the fluorescence signal last for 48 h (Fig. S11A-B). This long-term accumulation in the LNs is critical for the trigger of antigen-specific immune responses [36]. Additionally, the draining lymph nodes and major organs of mice were isolated and imaged, and the *ex vivo* results showed obvious antigen accumulation in LNs, which were consistent with the results *in vivo* (Fig. S12C).

To further study the *in vivo* tumor challenge, a prophylactic model was established to evaluate whether the combination of prophylactic nanovaccine HM-OVA with NLG-919/BLZ-945 (in the formulation of B@HM/N@HM) could enhance the immune protection against an E.G7-OVA tumor. Mice were immunized three times with an interval of 10 days and the immunized mice were challenged with E.G7-OVA cells, which is derived from EL4 cells by transfection of the OVA gene, three weeks post the final immunization. After incubation of tumors for 6 days, B@HM/N@HM was administered intratumorally (Fig. 4A). Immunization with HM-OVA plussed BLZ-945 or NLG-919 exhibited a tendency towards a better tumor-preventive effect than immunization with HM-OVA alone. More importantly, for mice treated with the combination of HM-OVA with BLZ-945/NLG-919, their average tumor volume was much smaller than the other groups at all time points. In

contrast, soluble free OVA was almost ineffective in preventing tumor growth (Fig. 4C-D). Moreover, survival analysis indicated that mice treated with combination HM-OVA + BLZ-945/NLG-919 resulted in 100% survival 38 days after the tumor inoculation, with a survival rate of 60% at day 50 (Fig. 4B). These results suggested that combination of prophylactic nanovaccine HM-OVA with BLZ-945/NLG-919 prevented tumor growth and prolonged the survival of mice effectively in an antigen-specific manner.

3.5. *Nanovaccine elicited robust antigen-specific T Cell responses and remodeled immunosuppressive TME for effective immunotherapy*

The synergy obtained with the combination of prophylactic nanovaccine with BLZ-945/NLG-919 prompted the design of a therapeutic intervention strategy of BN@HM-OVA in E.G7-OVA tumor-bearing mice. Mice were randomly divided into eight groups and injected three times with an interval of 4 days (Fig. 5A), when the average tumor volume reached ~50 mm^3. For mice injected with saline or HM-OVA, the palpable tumors appeared on day 5 and increased rapidly. The N@HM and B@HM groups conferred a relatively minor degree of tumor growth inhibition compared with N@HM-OVA and B@HM-OVA groups, respectively. Notably, the occurrence of tumor was retarded and the tumor growth was further evidently suppressed in BN@HM-OVA treatment group (Fig. 5B,C,E,F), with negligible systemic toxicity (Fig. 5D and Figs. S17–18), which indicates the potential of BN@HN-OVA as a therapeutic cancer nanovaccine. Furthermore, to study the antitumor effects of nanovaccine, the tumor tissues were immunostained with terminal deoxynucleotidyl transferase-mediated dUTP-biotin nick end labeling (TUNEL) and Ki-67 antigen to investigate the apoptosis and proliferation of tumor cells. It was observed that massive apoptosis and extremely few proliferation in the tumor sections from BN@HM-OVA treatment group (Fig. S15-16). All these histopathological analyses suggested that the potential of BN@HM-OVA as a therapeutic cancer vaccine, owing to the increased T cell tumor infiltration induced by it, followed by massive apoptosis of cancer cells.

Under cancer-associated inflammation, IDO is overexpressed and caused unavailability of tryptophan and accumulation of kynurenine in TME, which blunt the proliferation of cytotoxic T lymphocytes (CTLs, $CD3^+CD8^+$), while facilitating the growth of regulatory T cells (Tregs, $CD3^+CD4^+Foxp3^+$) [7,37,38]. Moreover, infiltration M2-like TAMs in TME regularly correlates with the CTLs suppression involving the inhibition of T-cell infiltration and CTL activity [39–41]. This imbalance promoted an immunosuppressive TME. Considering the ability of NLG-919 and BLZ-945 to inhibit IDO and M2-like TAMs activity, respectively, tumors obtained from the treated mice were harvested to analyze the immunological response using flow cytometry. The mice treated with HM-OVA alone or combination with NLG-919 had higher levels of M2-like TAMs ($CD206^{hi}CD11b^+F4/80^+$) and lower levels of M1-like TAMs ($CD80^{hi}CD11b^+F4/80^+$) [42] compared to the BLZ-945-added groups. Mice injected with BN@HM-OVA had the highest level of M1-like TAMs and the lowest level of M2-like TAMs (Fig. 6A,B,E and Fig. S13). Furthermore, a reduction of IL-10 (the

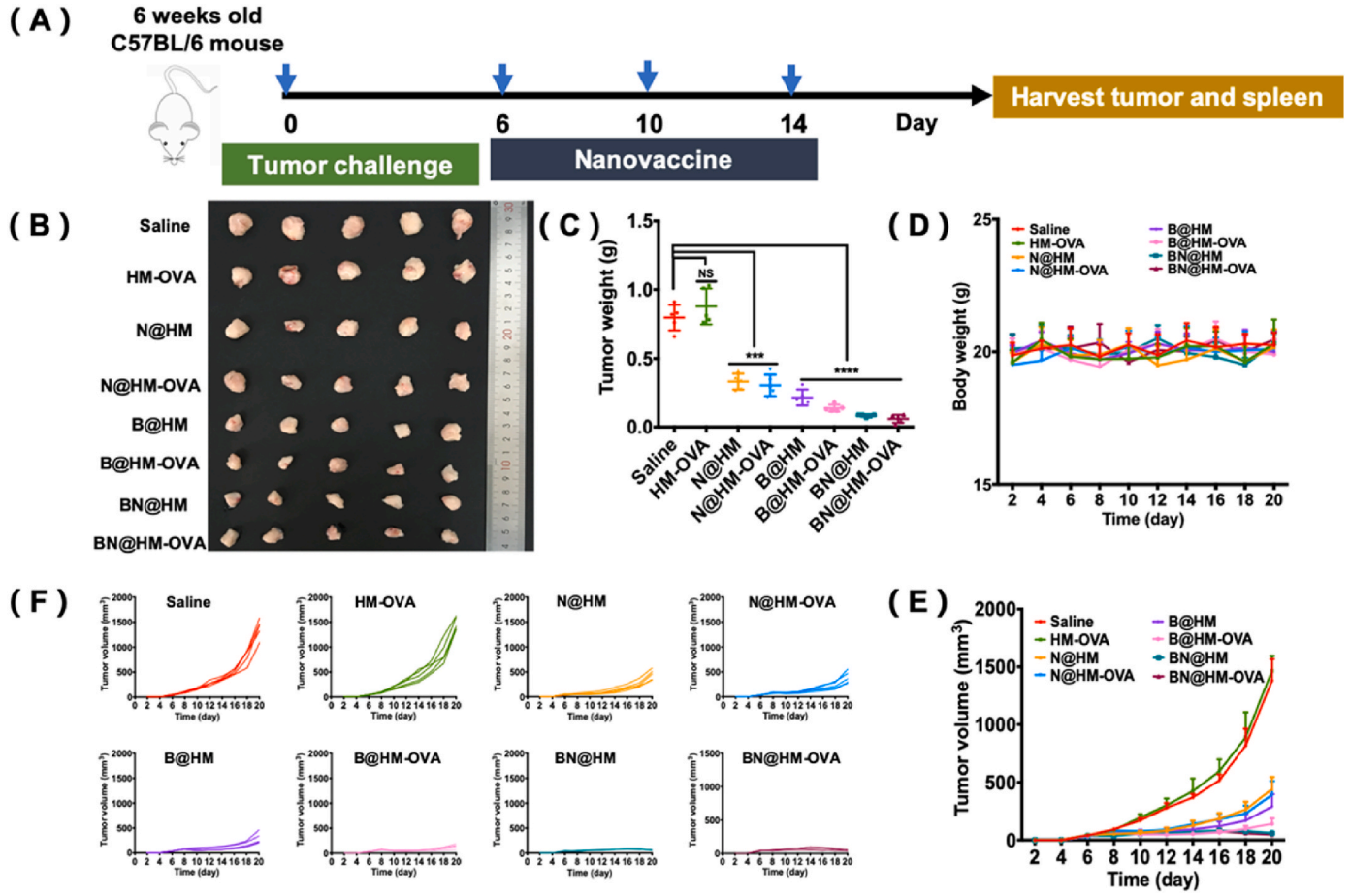

Fig. 5. Antitumor therapeutic effect of BN@HM-OVA nanovaccine in an established tumor model. (A) Scheme of tumor challenge experiment design. (B) Photograph of E.G7-OVA tumors from mice after various treatment (n = 5 biologically independent mice for each group). (C) Weights of E.G7-OVA tumors. (n = 5 biologically independent mice for each group). (D) Body weights of E.G7-OVA tumor-bearing mice after different treatment (n = 5 biologically independent mice for each group). (E) Average tumor growth curves (n = 5 biologically independent mice for each group). (F) Individual tumor growth curves in (E). Data are presented as mean ± SD. Statistical significance was calculated by one-way ANOVA (p values: ***$p < 0.001$ and ****$p < 0.0001$, NS: not significant).

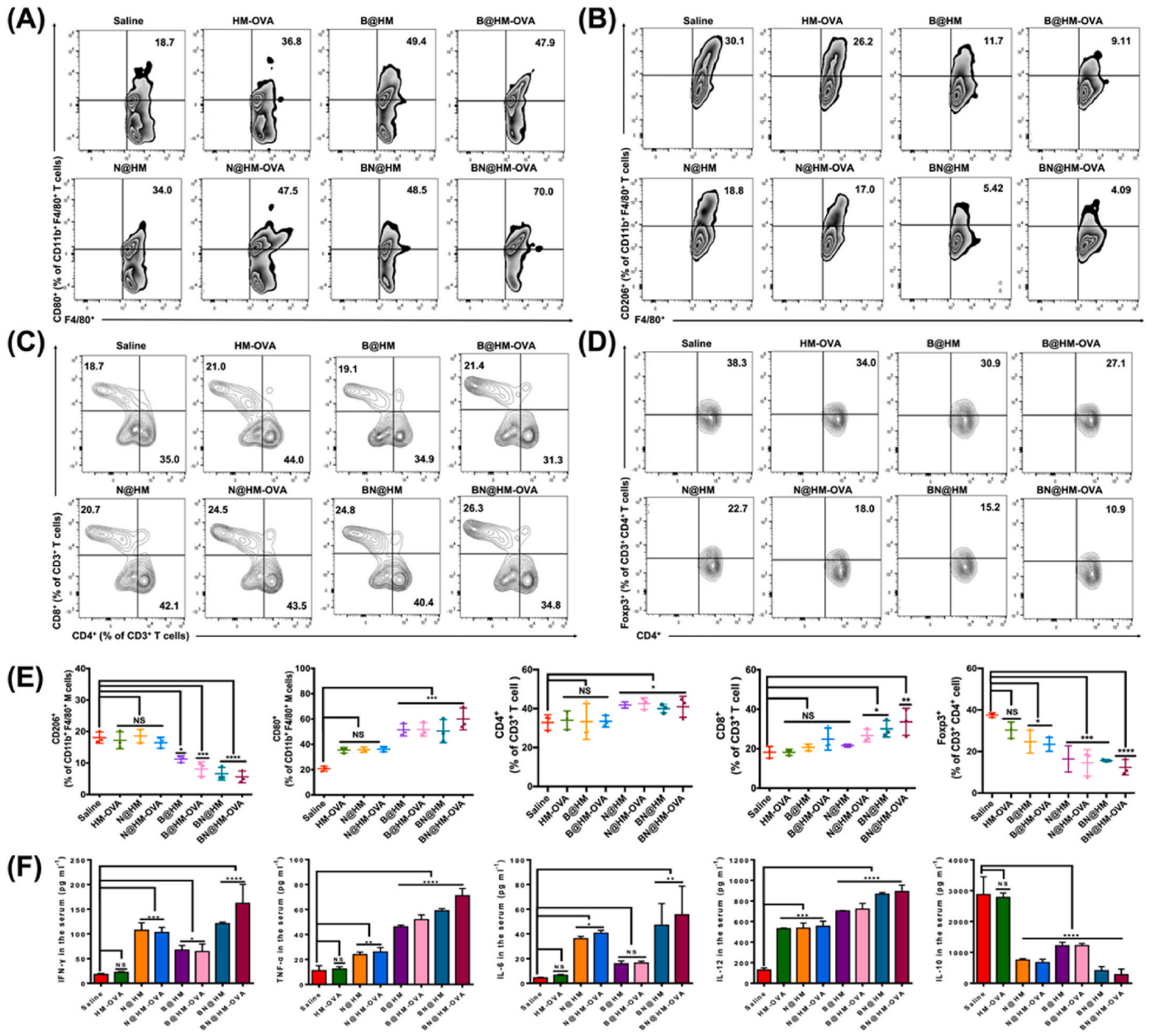

Fig. 6. BN@HM-OVA nanovaccine for triggering antitumor immune response and reprogramming immunosuppressive TME. Tumors were collected from mice after various treatment. (A) Representative flow cytometric analysis images of M1-like macrophages (CD80hi) and M2-like macrophages (CD206hi) (B) gating on F4/80$^+$CD11b$^+$ cells. (n = 3 biologically independent mice for each group). (C) Representative flow cytometric analysis of CD4+/CD8+ T cell populations gating on CD3$^+$ cells in tumor. (n = 3 biologically independent mice for each group). (D) Representative flow cytometric analysis of Foxp3$^+$CD4$^+$ T cell populations gating on CD3$^+$ cells in tumor. (n = 3 biologically independent mice for each group). (E) Corresponding quantitative results of M1/M2-like macrophages gating on F4/80$^+$CD11b$^+$ cells, CD4$^+$, CD8$^+$ and Focp3$^+$CD4$^+$ T cells gating on CD3$^+$ cells in (A), (B), (C) and (D). (F) Cytokine levels (IFN-γ, TNF-α, IL-6, IL-12, IL-10) in the serum from mice isolated after various treatments (n = 3 biologically independent mice for each group). Data are presented as mean ± SD. Statistical significance was calculated by one-way ANOVA (p values: *p < 0.05, **p < 0.01, ***p < 0.001 and ****p < 0.0001, NS: not significant).

pre-dominant cytokine secreted by M2 macrophages) an increase of IL-12 (the predominant cytokine secreted by M1 macrophages) in the plasma of corresponding mice detected by ELISA kits confirmed above results (Fig. 6F). The observed increase in IL-12 and decrease in IL-10 could be attributed to the successful depleting of M2-like macrophages.

Helper T (Th, CD3$^+$CD4$^+$) lymphocytes play an important role in helping B cells to regulate adaptive immunity, while CTLs directly kill cancer cells. In general, both CTLs and Th cells are crucial to trigger an effective immune response and achieve immune prevention and protection [43,44]. The groups added NLG-919 induced more CD4$^+$ T cells and tumor-infiltrating CD8$^+$ CTLs within the tumors than NLG-919-free groups. Remarkably, the most significant rise in the proportions of CD4$^+$ and CD8$^+$ T cells was observed in mice treated with BN@HM-OVA as compared to other groups (Fig. 6C,E and Fig. S14). Similarly, these results were further confirmed by the increase in IFN-γ (a predictor of antigen-specific CD8$^+$ CTLs-mediated responses), and tumor necrosis factor-α (TNF-α) in the plasma (Fig. 6F) [45,46]. Additionally, the infiltration of Tregs decreased dramatically in the group treated with BN@HM-OVA (Fig. 6D,E), as well as an increase in IL-6 (the cytokine involved in T-cell recruitment and differentiation, and in the suppression of Tregs) (Fig. 6F) [47,48]. The BN@HM-OVA displayed an increased infiltration of effector T cell, while a reduced infiltration of Tregs cells, which could be ascribed to modulation of the immunosuppressive TME that normally favors Tregs. Compared with the single

method of remodeling immunosuppressive TME, the combination of multiple targets provides a more effective strategy. Collectively, these results indicated that BN@HM-OVA nanovaccine not only can elicit robust innate and adaptive immune responses, but also remodeled the immunosuppressive TME to achieve antitumor efficacy. Although the effective antitumor resulted from high infiltration of activated $CD8^+$ T cell and the secretion of IFN-γ, the increase of IFN-γ subsequently induce the overexpression of programmed cell death-ligand 1 (PD-L1) on E.G7-OVA tumor cells [49]. Interaction of PD-L1 and programmed cell death-1 (PD-1) expressed by tumor-infiltrating T cells lead to an impaired function of $CD8^+$ T cells [50–52]. This mechanism urged a strategy of combination of nanovaccine with an immune checkpoint blockade (ICB).

3.6. *Sequential treatment with nanovaccine and anti-PD-1 antibody significantly improves the anticancer efficiency*

Despite the widespread applications of ICB monotherapy, the low durable response rate and resistance of anti-PD-1/PD-L1 therapy still exist in some cases [1,53]. The major reason attributed to the

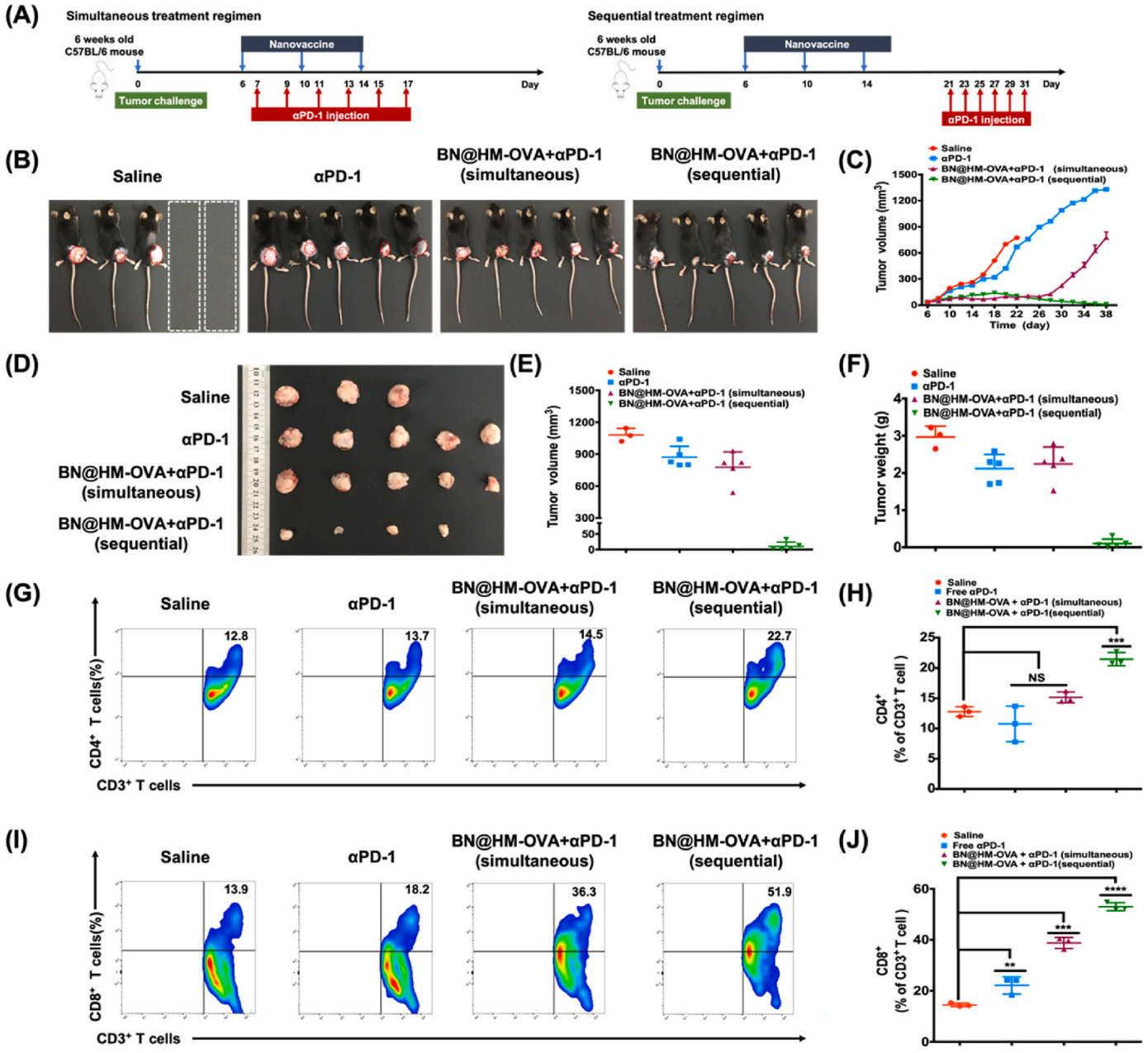

Fig. 7. Sequential treatment of BN@HM-OVA nanovaccine and αPD-1 restricts tumor growth more strongly than a simultaneous treatment regimen. (A) scheme of combination treatment regimen schedule. Simultaneous administration of the BN@HM-OVA nanovaccine and αPD-1 or sequential administration of the BN@HM-OVA nanovaccine followed by αPD-1 with a delay of days. (B) Representative photographs of mice after various treatments. The white dashed box indicates the mice that died before the end of the treatment regimen and the red dashed circles highlight the tumor site. (C) Average tumor growth curves. (n = 5 biologically independent mice for each group). (D) Photograph of E.G7-OVA tumors from mice after various treatment. (n = 5 biologically independent mice for each group). (E) Volume and Weight (F) of E.G7-OVA tumors. (n = 5 biologically independent mice for each group). (G) Representative flow cytometric analysis of $CD4^+$ and $CD8^+$ (I) T cell populations gating on $CD3^+$ cells in tumor. (n = 3 biologically independent mice for each group). (H) Corresponding quantitative results of $CD4^+$ (H) and $CD8^+$ (J) T cells gating on $CD3^+$ cells in (G) and (I). Data are presented as mean ± SD. Statistical significance was calculated by one-way ANOVA (p values: $^{**}p < 0.01$, $^{***}p < 0.001$ and $^{****}p < 0.0001$, NS: not significant).

phenomenon is the lack of infiltrating $CD8^+$ T cells in tumor tissues [3, 54]. The aforementioned results have confirmed that proportion of tumor-infiltrating $CD8^+$ T cells was raised in mice treated with BN@HM-OVA (Fig. 6C), thus antitumor efficiency of the combination of BN@HM-OVA and anti-PD-1 (αPD-1) was assessed in a therapeutic model. However, a recent study found that PD-1 blockade before antigen priming results in increased antigen-specific $CD8^+$ T cell apoptosis and abrogates the antitumor ability of the combination of nanovaccine and αPD-1 [4]. Therefore, an appropriate treatment sequence of nanovaccine and αPD-1 is important in determining the therapeutic efficiency. Finally, two combination treatment regimens were established: (1) simultaneous injection of the nanovaccine and αPD-1; (2) sequential injection of nanovaccine followed by αPD-1 with 1-week delay (Fig. 7A). For the simultaneous treatment regimen, mice inoculated with E.G7-OVA tumor were simultaneously injected with BN@HM-OVA and αPD-1. For the sequential treatment regimen, one week after the last injection of nanovaccine, αPD-1 administration started. For the saline- and αPD-1-treated groups, the tumor volume increased rapidly and reached about 1000 mm^3 within 21 days, suggesting the inefficiency of inhibiting tumor growth in αPD-1 alone treatment group (Fig. 7B-F). Although PD-1 blockade, when initiated simultaneously with nanovaccine inhibited tumor growth through day 22, the tumor recurred after the end of αPD-1 administration (Fig. 7C). Notably, the tumor occurring was continuously restricted by sequential injection of nanovaccine followed by αPD-1 with a delay, especially showing that 20.0% of mice were tumor-free on the end of treatment (Fig. 7B,D). Moreover, compared with the previous group (Fig. 5E) using BN@HM-OVA alone in the therapeutic model, it showed superior and more sustained ability of tumor inhibition. Furthermore, immune response results including the number of activated $CD4^+$ T cells and $CD8^+$ CTLs indicated that sequential treatment regimen dramatically increased proportions of $CD8^+$ T and $CD4^+$ T cells infiltration in tumor tissues (Fig. 7G-J , Fig. S19). Taken together, these results demonstrated that the sequential administration of nanovaccine and αPD-1 stimulated $CD8^+$ T cells properly and subsequently result in potent antitumor immune response.

4. Conclusions

In the present work, we constructed a pH-sensitive antitumor nanovaccine with efficient antigen delivery as well as synergistic immunotherapy of E.G7-OVA tumors. Importantly, such size adjustable and zeta potential transitional nanovaccine significantly accelerate OVA antigen internalization into DCs and enables precisely controllable drug release of BLZ-945 and NLG-919 into TME. Subsequently, the bioactive nanovaccine of BM@HM-OVA exhibited superior ability to induce DCs maturation and robust antigen-specific T cell responses over other formulations both *in vitro* and *in vivo*. In addition, the antitumor synergism of the bioactive nanovaccine with BLZ-945/NLG-919 immune therapy not only prevent antigen-expressing E.G7 tumors growth on a prophylactic model, but also prohibited tumor progression and prolong animal survival on the therapeutic model. Furthermore, based on optimal timing and sequencing of PD-1 antibody blockade with respect to T cell receptor (TCR) activated by the bioactive nanovaccine, the combination treatment of BN@HM-OVA and αPD-1was adopted, which achieved maximum therapeutic benefits. Taken together, the improved antitumor performance obtained with the bioactive nanovaccine resulted from the amelioration of immune-suppressive TME, which in turn enhanced DCs recruitment, differentiation, subsequent antigen presentation and T-cells responses. These results indicate that the novel treatment regimens and combined immunotherapy used in the bioactive nanovaccine platform will extend its application in the therapy of other solid tumors.

CRediT authorship contribution statement

Xiaoxue Xie: Conceptualization, Methodology, Software, Validation, Formal analysis, Investigation, Resources, Data curation, Writing – original draft, Writing – review & editing. **Yi Feng:** Data curation, Investigation. **Hanxi Zhang:** Formal analysis, Investigation. **Qingqing Su:** Formal analysis, Investigation, Data curation. **Ting Song:** Formal analysis, Investigation, Data curation. **Geng Yang:** Investigation, Resources, Data curation. **Ningxi Li:** Investigation, Resources, Data curation. **Xiaodan Wei:** Investigation, Resources, Data curation. **Tingting Li:** Writing – review & editing, Visualization, Supervision. **Xiang Qin:** Writing – review & editing, Visualization, Supervision. **Shun Li:** Writing – review & editing, Visualization, Supervision. **Chunhui Wu:** Writing – review & editing, Visualization, Supervision. **Xiaojuan Zhang:** Investigation, Resources, Data curation. **Guixue Wang:** Conceptualization, Writing – review & editing, Visualization, Supervision, Project administration, Funding acquisition. **Yiyao Liu:** Conceptualization, Writing – review & editing, Visualization, Supervision, Project administration, Funding acquisition. **Hong Yang:** Conceptualization, Writing – review & editing, Visualization, Supervision, Project administration, Funding acquisition.

Declaration of competing interest

The authors declare that they have no known competing financial interests or personal relationships that could have appeared to influence the work reported in this paper.

Acknowledgments

This research was supported, in part or in whole, by the National Natural Science Foundation of China (U19A2006, 12132004, 12032007, 11972111, 31900940, 32071304, 32171309, 32171395), the Sichuan Science and Technology Program (21YJ0130), the Joint Funds of Center for Engineering Medicine (ZYGX2021YGLH010, ZYGX2021YGLH017, ZYGX2021YGLH023), and the technical support from the Public Experiment Centre of State Bioindustrial Base (Chongqing).

Appendix A. Supplementary data

Supplementary data to this article can be found online at https://doi.org/10.1016/j.bioactmat.2022.03.008.

References

[1] A.B. El-Khoueiry, B. Sangro, T. Yau, T.S. Crocenzi, M. Kudo, C. Hsu, T.Y. Kim, S. P. Choo, J. Trojan, T.H.R. Welling, T. Meyer, Y.K. Kang, W. Yeo, A. Chopra, J. Anderson, C. Dela Cruz, L. Lang, J. Neely, H. Tang, H.B. Dastani, I. Melero, Nivolumab in patients with advanced hepatocellular carcinoma (CheckMate 040): an open-label, non-comparative, phase 1/2 dose escalation and expansion trial, Lancet 389 (10088) (2017) 2492–2502.
[2] J. Zhang, F. Dang, J. Ren, W. Wei, Biochemical aspects of PD-L1 regulation in cancer immunotherapy, Trends Biochem. Sci. 43 (12) (2018) 1014–1032.
[3] P. Sharma, S. Hu-Lieskovan, J.A. Wargo, A. Ribas, Primary, adaptive, and acquired resistance to cancer immunotherapy, Cell 168 (4) (2017) 707–723.
[4] V. Verma, R.K. Shrimali, S. Ahmad, W. Dai, H. Wang, S. Lu, R. Nandre, P. Gaur, J. Lopez, M. Sade-Feldman, K. Yizhak, S.L. Bjorgaard, K.T. Flaherty, J.A. Wargo, G. M. Boland, R.J. Sullivan, G. Getz, S.A. Hammond, M. Tan, J. Qi, P. Wong, T. Merghoub, J. Wolchok, N. Hacohen, J.E. Janik, M. Mkrtichyan, S. Gupta, S. N. Khleif, PD-1 blockade in subprimed CD8 cells induces dysfunctional PD-1(+) CD38(hi) cells and anti-PD-1 resistance, Nat. Immunol. 20 (9) (2019) 1231–1243.
[5] J.R. Moffett, M.A. Namboodiri, Tryptophan and the immune response, Immunol. Cell Biol. 81 (4) (2003) 247–265.
[6] C. Uyttenhove, L. Pilotte, I. Theate, V. Stroobant, D. Colau, N. Parmentier, T. Boon, B.J. Van den Eynde, Evidence for a tumoral immune resistance mechanism based on tryptophan degradation by indoleamine 2,3-dioxygenase, Nat. Med. 9 (10) (2003) 1269–1274.
[7] S.R. Selvan, J.P. Dowling, W.K. Kelly, J. Lin, Indoleamine 2,3-dioxygenase (Ido): biology and target in cancer immunotherapies, Curr. Cancer Drug Targets 16 (9) (2016) 755–764.
[8] A. Mantovani, S. Sozzani, M. Locati, P. Allavena, A. Sica, Macrophage polarization: tumor-associated macrophages as a paradigm for polarized M2 mononuclear phagocytes, Trends Immunol. 23 (11) (2002) 549–555.
[9] E.Y. Lin, J.W. Pollard, Tumor-associated macrophages press the angiogenic switch in breast cancer, Cancer Res. 67 (11) (2007) 5064–5066.
[10] W. Li, J. Yang, L. Luo, M. Jiang, B. Qin, H. Yin, C. Zhu, X. Yuan, J. Zhang, Z. Luo, Y. Du, Q. Li, Y. Lou, Y. Qiu, J. You, Targeting photodynamic and photothermal

therapy to the endoplasmic reticulum enhances immunogenic cancer cell death, Nat. Commun. 10 (1) (2019) 3349.
[11] L. Huang, Y. Li, Y. Du, Y. Zhang, X. Wang, Y. Ding, X. Yang, F. Meng, J. Tu, L. Luo, C. Sun, Mild photothermal therapy potentiates anti-PD-L1 treatment for immunologically cold tumors via an all-in-one and all-in-control strategy, Nat. Commun. 10 (1) (2019) 4871.
[12] E.S. Nakasone, H.A. Askautrud, T. Kees, J.H. Park, V. Plaks, A.J. Ewald, M. Fein, M. G. Rasch, Y.X. Tan, J. Qiu, J. Park, P. Sinha, M.J. Bissell, E. Frengen, Z. Werb, M. Egeblad, Imaging tumor-stroma interactions during chemotherapy reveals contributions of the microenvironment to resistance, Cancer Cell 21 (4) (2012) 488–503.
[13] D.A. Hume, K.P. MacDonald, Therapeutic applications of macrophage colony-stimulating factor-1 (CSF-1) and antagonists of CSF-1 receptor (CSF-1R) signaling, Blood 119 (8) (2012) 1810–1820.
[14] I. Ott, H. Scheffler, R. Gust, Development of a method for the quantification of the molar gold concentration in tumour cells exposed to gold-containing drugs, ChemMedChem 2 (5) (2007) 702–707.
[15] D. Cao, X. Ma, J. Cai, J. Luan, A.J. Liu, R. Yang, Y. Cao, X. Zhu, H. Zhang, Y. X. Chen, Y. Shi, G.X. Shi, D. Zou, X. Cao, M.J. Grusby, Z. Xie, W.J. Zhang, ZBTB20 is required for anterior pituitary development and lactotrope specification, Nat. Commun. 7 (2016) 11121.
[16] S. Spranger, R.M. Spaapen, Y. Zha, J. Williams, Y. Meng, T.T. Ha, T.F. Gajewski, Up-regulation of PD-L1, Ido, and T(regs) in the melanoma tumor microenvironment is driven by CD8(+) T cells, Sci. Transl. Med. 5 (200) (2013) 200ra116.
[17] V. Verma, R.K. Shrimali, S. Ahmad, W. Dai, H. Wang, S. Lu, R. Nandre, P. Gaur, J. Lopez, M. Sade-Feldman, K. Yizhak, S.L. Bjorgaard, K.T. Flaherty, J.A. Wargo, G. M. Boland, R.J. Sullivan, G. Getz, S.A. Hammond, M. Tan, J. Qi, P. Wong, T. Merghoub, J. Wolchok, N. Hacohen, J.E. Janik, M. Mkrtichyan, S. Gupta, S. N. Khleif, Author Correction: PD-1 blockade in subprimed CD8 cells induces dysfunctional PD-1(+)CD38(hi) cells and anti-PD-1 resistance, Nat. Immunol. 20 (11) (2019) 1555.
[18] Y.L. Chiu, S.A. Chen, J.H. Chen, K.J. Chen, H.L. Chen, H.W. Sung, A dual-emission Forster resonance energy transfer nanoprobe for sensing/imaging pH changes in the biological environment, ACS Nano 4 (12) (2010) 7467–7474.
[19] X. Han, D.E. Liu, T. Wang, H. Lu, J. Ma, Q. Chen, H. Gao, Aggregation-induced-emissive molecule incorporated into polymeric nanoparticulate as FRET donor for observing doxorubicin delivery, ACS Appl. Mater. Interfaces 7 (42) (2015) 23760–23766.
[20] X. Xie, Y. Chen, Z. Chen, Y. Feng, J. Wang, T. Li, S. Li, X. Qin, C. Wu, C. Zheng, J. Zhu, F. You, Y. Liu, H. Yang, Polymeric hybrid nanomicelles for cancer theranostics: an efficient and precise anticancer strategy for the codelivery of doxorubicin/miR-34a and magnetic resonance Imaging, ACS Appl. Mater. Interfaces 11 (47) (2019) 43865–43878.
[21] D. Wu, J. Zhou, X. Chen, Y. Chen, S. Hou, H. Qian, L. Zhang, G. Tang, Z. Chen, Y. Ping, W. Fang, H. Duan, Mesoporous polydopamine with built-in plasmonic core: traceable and NIR triggered delivery of functional proteins, Biomaterials 238 (2020) 119847.
[22] K. Palucka, J. Banchereau, Cancer immunotherapy via dendritic cells, Nat. Rev. Cancer 12 (4) (2012) 265–277.
[23] A.L. Mellor, D.H. Munn, Tryptophan catabolism and T-cell tolerance: immunosuppression by starvation? Immunol. Today 20 (10) (1999) 469–473.
[24] Y. Chen, R. Xia, Y. Huang, W. Zhao, J. Li, X. Zhang, P. Wang, R. Venkataramanan, J. Fan, W. Xie, X. Ma, B. Lu, S. Li, An immunostimulatory dual-functional nanocarrier that improves cancer immunochemotherapy, Nat. Commun. 7 (2016) 13443.
[25] B. Molon, B. Cali, A. Viola, T cells and cancer: how metabolism shapes immunity, Front. Immunol. 7 (2016) 20.
[26] L.E. Paulis, S. Mandal, M. Kreutz, C.G. Figdor, Dendritic cell-based nanovaccines for cancer immunotherapy, Curr. Opin. Immunol. 25 (3) (2013) 389–395.
[27] A. Lanzavecchia, F. Sallusto, Regulation of T cell immunity by dendritic cells, Cell 106 (3) (2001) 263–266.
[28] O. Dienz, M. Rincon, The effects of IL-6 on CD4 T cell responses, Clin. Immunol. 130 (1) (2009) 27–33.
[29] J. Xu, J. Lv, Q. Zhuang, Z. Yang, Z. Cao, L. Xu, P. Pei, C. Wang, H. Wu, Z. Dong, Y. Chao, C. Wang, K. Yang, R. Peng, Y. Cheng, Z. Liu, A general strategy towards personalized nanovaccines based on fluoropolymers for post-surgical cancer immunotherapy, Nat. Nanotechnol. 15 (12) (2020) 1043–1052.
[30] D.G. DeNardo, D.J. Brennan, E. Rexhepaj, B. Ruffell, S.L. Shiao, S.F. Madden, W. M. Gallagher, N. Wadhwani, S.D. Keil, S.A. Junaid, H.S. Rugo, E.S. Hwang, K. Jirstrom, B.L. West, L.M. Coussens, Leukocyte complexity predicts breast cancer survival and functionally regulates response to chemotherapy, Cancer Discov. 1 (1) (2011) 54–67.
[31] Y. Qian, S. Qiao, Y. Dai, G. Xu, B. Dai, L. Lu, X. Yu, Q. Luo, Z. Zhang, Molecular-targeted immunotherapeutic strategy for melanoma via dual-targeting nanoparticles delivering small Interfering RNA to tumor-associated macrophages, ACS Nano 11 (9) (2017) 9536–9549.
[32] C.H. Ries, M.A. Cannarile, S. Hoves, J. Benz, K. Wartha, V. Runza, F. Rey-Giraud, L. P. Pradel, F. Feuerhake, I. Klaman, T. Jones, U. Jucknischke, S. Scheiblich, K. Kaluza, I.H. Gorr, A. Walz, K. Abiraj, P.A. Cassier, A. Sica, C. Gomez-Roca, K. E. de Visser, A. Italiano, C. Le Tourneau, J.P. Delord, H. Levitsky, J.Y. Blay, D. Ruttinger, Targeting tumor-associated macrophages with anti-CSF-1R antibody reveals a strategy for cancer therapy, Cancer Cell 25 (6) (2014) 846–859.
[33] W. He, P. Liang, G. Guo, Z. Huang, Y. Niu, L. Dong, C. Wang, J. Zhang, Re-polarizing myeloid-derived suppressor cells (MDSCs) with cationic polymers for cancer immunotherapy, Sci. Rep. 6 (2016) 24506.
[34] H. Liu, K.D. Moynihan, Y. Zheng, G.L. Szeto, A.V. Li, B. Huang, D.S. Van Egeren, C. Park, D.J. Irvine, Structure-based programming of lymph-node targeting in molecular vaccines, Nature 507 (7493) (2014) 519–522.
[35] G.J. Randolph, V. Angeli, M.A. Swartz, Dendritic-cell trafficking to lymph nodes through lymphatic vessels, Nat. Rev. Immunol. 5 (8) (2005) 617–628.
[36] S. De Koker, J. Cui, N. Vanparijs, L. Albertazzi, J. Grooten, F. Caruso, B.G. De Geest, Engineering polymer hydrogel nanoparticles for lymph node-targeted delivery, Angew Chem. Int. Ed. Engl. 55 (4) (2016) 1334–1339.
[37] J. Lu, X. Liu, Y.P. Liao, X. Wang, A. Ahmed, W. Jiang, Y. Ji, H. Meng, A.E. Nel, Breast cancer chemo-immunotherapy through liposomal delivery of an immunogenic cell death stimulus plus interference in the Ido-1 pathway, ACS Nano 12 (11) (2018) 11041–11061.
[38] J. Peng, Y. Xiao, W. Li, Q. Yang, L. Tan, Y. Jia, Y. Qu, Z. Qian, Photosensitizer micelles together with Ido inhibitor enhance cancer photothermal therapy and immunotherapy, Adv. Sci. 5 (5) (2018) 1700891.
[39] A. Mantovani, P. Allavena, The interaction of anticancer therapies with tumor-associated macrophages, J. Exp. Med. 212 (4) (2015) 435–445.
[40] C. Baer, M.L. Squadrito, D. Laoui, D. Thompson, S.K. Hansen, A. Kiialainen, S. Hoves, C.H. Ries, C.H. Ooi, M. De Palma, Suppression of microRNA activity amplifies IFN-gamma-induced macrophage activation and promotes anti-tumour immunity, Nat. Cell Biol. 18 (7) (2016) 790–802.
[41] S.M. Pyonteck, L. Akkari, A.J. Schuhmacher, R.L. Bowman, L. Sevenich, D.F. Quail, O.C. Olson, M.L. Quick, J.T. Huse, V. Teijeiro, M. Setty, C.S. Leslie, Y. Oei, A. Pedraza, J. Zhang, C.W. Brennan, J.C. Sutton, E.C. Holland, D. Daniel, J. A. Joyce, CSF-1R inhibition alters macrophage polarization and blocks glioma progression, Nat. Med. 19 (10) (2013) 1264–1272.
[42] Q. Chen, C. Wang, X. Zhang, G. Chen, Q. Hu, H. Li, J. Wang, D. Wen, Y. Zhang, Y. Lu, G. Yang, C. Jiang, J. Wang, G. Dotti, Z. Gu, In situ sprayed bioresponsive immunotherapeutic gel for post-surgical cancer treatment, Nat. Nanotechnol. 14 (1) (2019) 89–97.
[43] Q. Chen, L. Xu, C. Liang, C. Wang, R. Peng, Z. Liu, Photothermal therapy with immune-adjuvant nanoparticles together with checkpoint blockade for effective cancer immunotherapy, Nat. Commun. 7 (2016) 13193.
[44] S. Stenger, D.A. Hanson, R. Teitelbaum, P. Dewan, K.R. Niazi, C.J. Froelich, T. Ganz, S. Thoma-Uszynski, A. Melian, C. Bogdan, S.A. Porcelli, B.R. Bloom, A. M. Krensky, R.L. Modlin, An antimicrobial activity of cytolytic T cells mediated by granulysin, Science 282 (5386) (1998) 121–125.
[45] L. Zhang, S. Wu, Y. Qin, F. Fan, Z. Zhang, C. Huang, W. Ji, L. Lu, C. Wang, H. Sun, X. Leng, D. Kong, D. Zhu, Targeted codelivery of an antigen and dual agonists by hybrid nanoparticles for enhanced cancer immunotherapy, Nano Lett. 19 (7) (2019) 4237–4249.
[46] D.W. Kowalczyk, A.P. Wlazlo, W. Giles-Davis, A.R. Kammer, S. Mukhopadhyay, H. C. Ertl, Vaccine-induced CD8+ T cells eliminate tumors by a two-staged attack, Cancer Gene Ther. 10 (12) (2003) 870–878.
[47] C. Pasare, R. Medzhitov, Toll-like receptors: balancing host resistance with immune tolerance, Curr. Opin. Immunol. 15 (6) (2003) 677–682.
[48] J. Scheller, A. Chalaris, D. Schmidt-Arras, S. Rose-John, The pro- and anti-inflammatory properties of the cytokine interleukin-6, Biochim. Biophys. Acta 1813 (5) (2011) 878–888.
[49] Y. Kim, S. Kang, H. Shin, T. Kim, B. Yu, J. Kim, D. Yoo, S. Jon, Sequential and timely combination of a cancer nanovaccine with immune checkpoint blockade effectively inhibits tumor growth and relapse, Angew Chem. Int. Ed. Engl. 59 (34) (2020) 14628–14638.
[50] G. Zhu, G.M. Lynn, O. Jacobson, K. Chen, Y. Liu, H. Zhang, Y. Ma, F. Zhang, R. Tian, Q. Ni, S. Cheng, Z. Wang, N. Lu, B.C. Yung, Z. Wang, L. Lang, X. Fu, A. Jin, I.D. Weiss, H. Vishwasrao, G. Niu, H. Shroff, D.M. Klinman, R.A. Seder, X. Chen, Albumin/vaccine nanocomplexes that assemble in vivo for combination cancer immunotherapy, Nat. Commun. 8 (1) (2017) 1954.
[51] S.L. Topalian, C.G. Drake, D.M. Pardoll, Targeting the PD-1/B7-H1(PD-L1) pathway to activate anti-tumor immunity, Curr. Opin. Immunol. 24 (2) (2012) 207–212.
[52] M.E. Keir, M.J. Butte, G.J. Freeman, A.H. Sharpe, PD-1 and its ligands in tolerance and immunity, Annu. Rev. Immunol. 26 (2008) 677–704.
[53] S.L. Topalian, M. Sznol, D.F. McDermott, H.M. Kluger, R.D. Carvajal, W. H. Sharfman, J.R. Brahmer, D.P. Lawrence, M.B. Atkins, J.D. Powderly, P. D. Leming, E.J. Lipson, I. Puzanov, D.C. Smith, J.M. Taube, J.M. Wigginton, G. D. Kollia, A. Gupta, D.M. Pardoll, J.A. Sosman, F.S. Hodi, Survival, durable tumor remission, and long-term safety in patients with advanced melanoma receiving nivolumab, J. Clin. Oncol. 32 (10) (2014) 1020–1030.
[54] D.M. Pardoll, The blockade of immune checkpoints in cancer immunotherapy, Nat. Rev. Cancer 12 (4) (2012) 252–264.